Supporting Information

Vacancy-Induced Anion and Cation Redox Chemistry in Cation-Defect F-doped Anatase TiO_2

Haoxin Li[ab], Yining Li[bc], Xiaolin Zhao[bc], Youwei Wang[bc], Kexian Huang[b], Wujie Qiu*[bc], Jifen Wang*[a] and Jianjun Liu*[bcd]

[a]School of Science, College of Art and Science, Shanghai Polytechnic University No. 2360 Jinhai Rd., Shanghai 201209, China

[b]State Key Laboratory of High Performance Ceramics and Superfine Microstructure, Shanghai Institute of Ceramics, Chinese Academy of Sciences, 1295 Dingxi Road, Shanghai 200050, China

[c]Center of Materials Science and Optoelectronics Engineering, University of Chinese Academy of Sciences, Beijing 100049, China

[d]School of Chemistry and Materials Science, Hangzhou Institute for Advanced Study, University of Chinese Academy of Science, 1 Sub-lane Xiangshan, Hangzhou, 310024, China

*Email: jliu@mail.sic.ac.cn; wjqiu1988@gmail.com; wangjifen@sspu.edu.cn

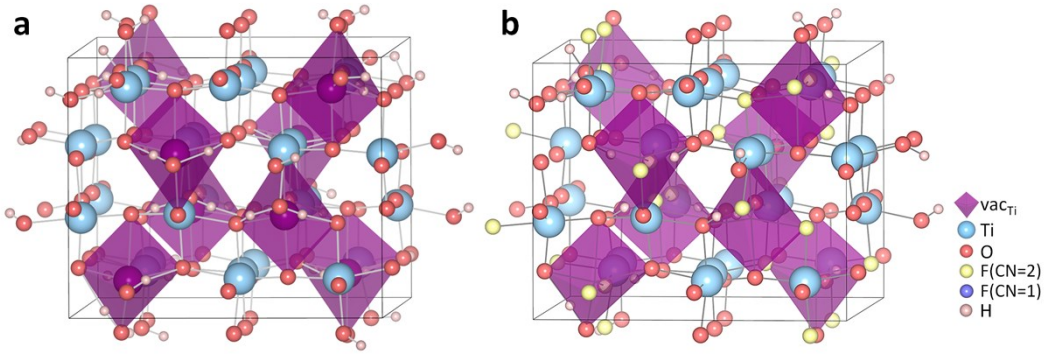

Fig. S1 (a) The structure of $Ti_{0.78}\square_{0.22}O_{1.11}(OH)_{0.89}$. (b) structure of $Ti_{0.78}\square_{0.22}O_{1.11}F_{0.44}(OH)_{0.44}$.

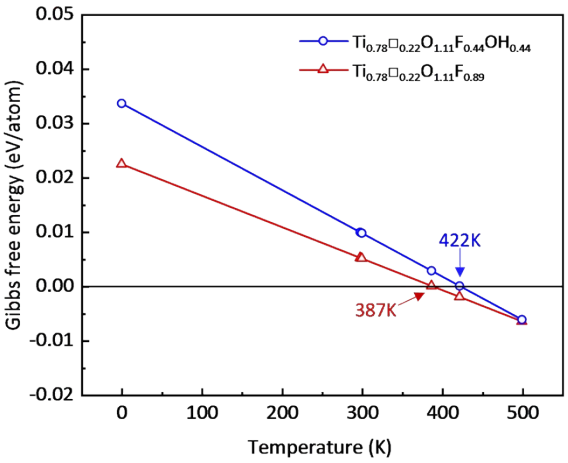

Fig. S2 Calculated temperature-dependent free energy of $Ti_{0.78}□_{0.22}O_{1.11}F_{0.89}$ (red line) and $Ti_{0.78}□_{0.22}O_{1.11}F_{0.44}(OH)_{0.44}$ (bule line) versus TiO_2, TiF_4 and H_2O phase mixtures.

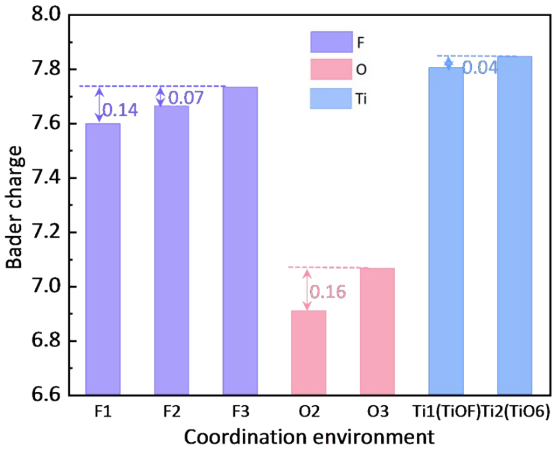

Fig. S3 Bader charge analysis of different local structures. F with three coordination positions, O with two coordination positions as and Ti with two regions.

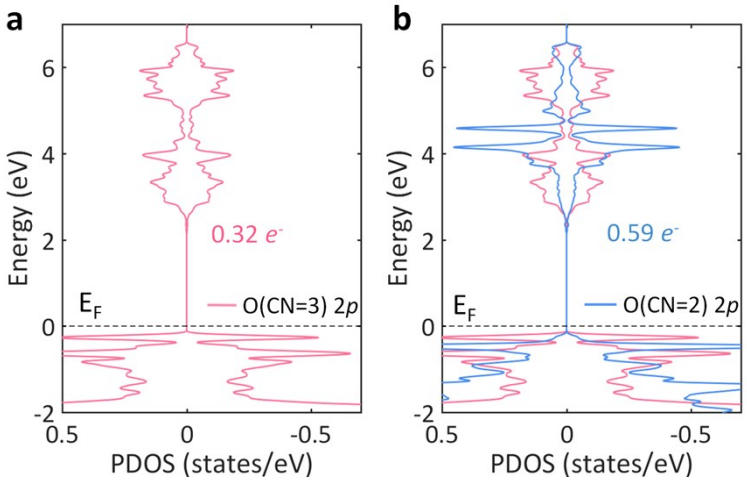

Fig. S4 Effects of different coordination environments on the electronic state of oxygen anions. The projected density of the O-2*p* orbital state density (pDOS) of O atoms in oxygen-doped defect titanium dioxide consists of different coordination (a) three coordination (b) two coordination.

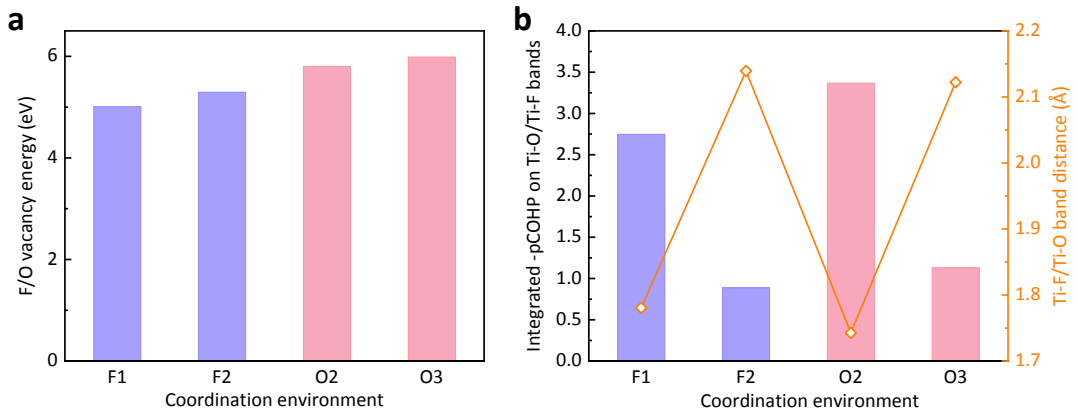

Fig. S5 Stability of oxidation state F and O. (a) The vacancy formation energy of oxygen or fluorine atoms. (b) The integration of the projection crystal orbital Hamiltonian population (ICOHP) shows Ti-O/Ti-F bond strength.

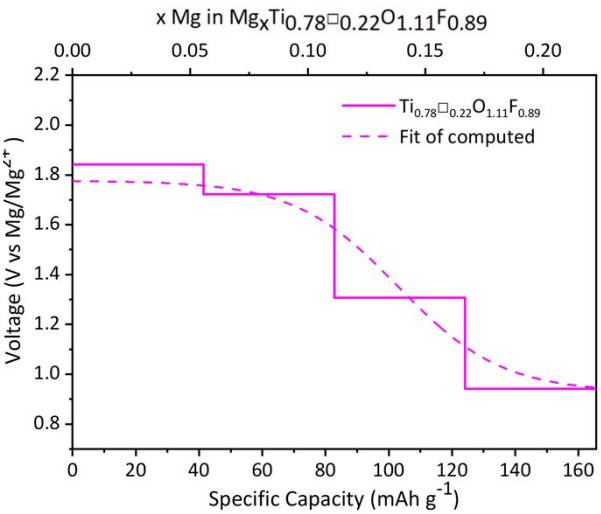

Fig. S6 Calculated voltage plateaus of Mg^{2+} insertion and the fitting voltage curve.

Table S1. The calculation details of the chemical potential in the solid-phase method. Experimental values, calculated values and equations of TiO_2, TiF_3 and Ti.

Compounds	E_{DFT}(GGA)	$\Delta G_r(Expt)$ (kJ/mol)
TiO_2	-26.90	-833.266
TiF_3	-27.09	-1361.864
Ti	-7.85	0
Equation(I)	$\mu_{O_2} = E^{TiO_2}(GGA) - E^{Ti}(GGA) - \Delta G_r^O(Expt)$ (eV)	
Equation(II)	$\mu_{F_2} = \frac{3}{2}\{E^{TiF_3}(GGA) - E^{Ti}(GGA) - \Delta G_r^F(Expt)\}$ (eV)	

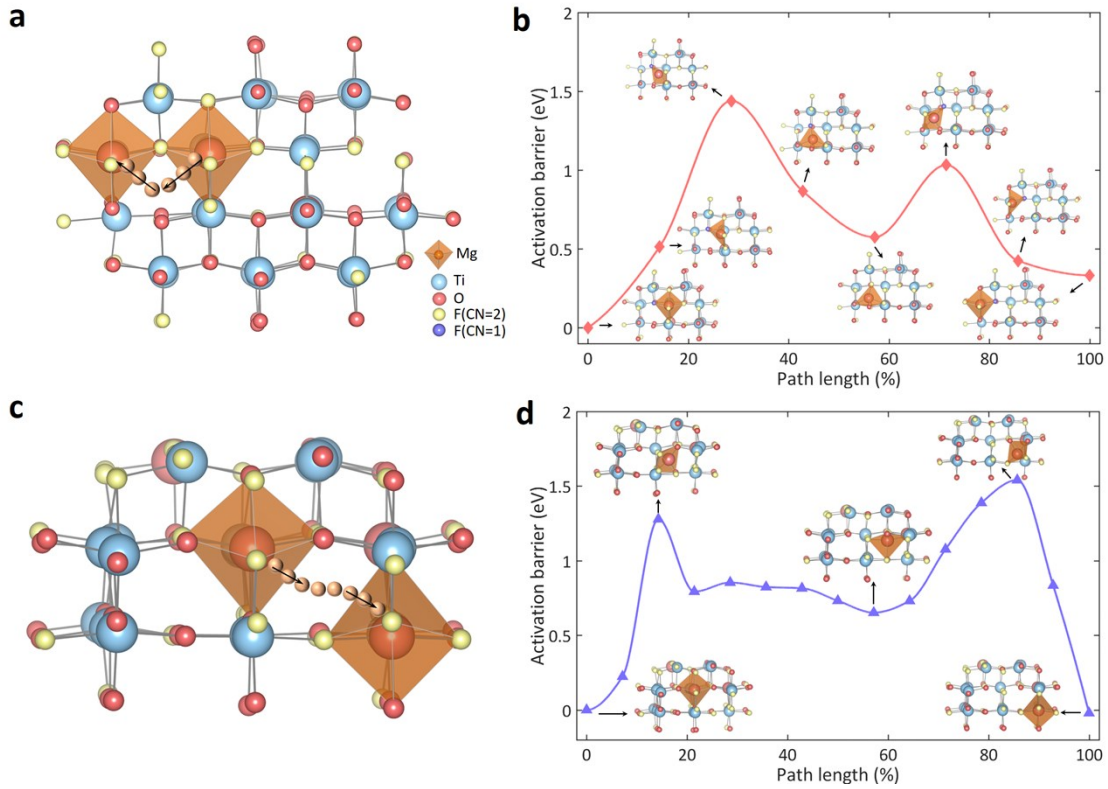

Fig. S7 The a and b are the Mg migration paths in scattered-defect structures, c and d are Mg migration paths in connected-defect structures.

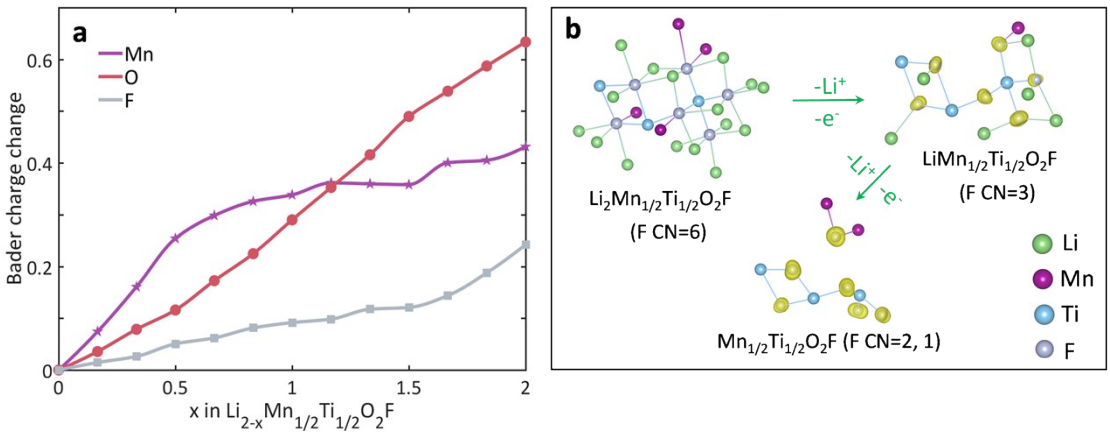

Fig. S8 Electrochemical characteristics of $Li_2Ti_{0.5}Mn_{0.5}O_2F$. (a) Average change of bader charge during delithiation. (b) The evolution of F coordination number in the process of delithiation.